Food & Function

ROYAL SOCIETY OF CHEMISTRY

PAPER

View Article Online
View Journal

Cite this: DOI: 10.1039/d5fo03232f

Noni (*Morinda citrifolia* L.) fruit juice induces ferroptosis in gastric cancer cells *via* the Nrf2/HO-1–GPX4 axis

Zhihao Xie, *† Hejiao Li,† Weifeng Lu, * Lijie Liu, Dianxiao Liao, Chunmeng Mai, Xian Fu, Minni Zhang, Xiuying Tian, Xinbao Hao * and Lu Xu *

Noni (*Morinda citrifolia* L.) is a natural dietary therapeutic plant native to the selenium-rich tropical region of Chengmai, Hainan, China. It exhibits anti-tumor, anti-aging, and lipid-lowering properties; however, the precise mechanism by which it inhibits cancer progression remains unclear. This study investigates the mechanism by which noni juice targets ferroptosis in gastric cancer (GC) and analyzes its bioactive components. First, the efficacy of noni juice was evaluated using an *in vivo* orthotopic gastric cancer model, while its blood-absorbed components were analyzed *via* UPLC-Q Exactive MS. Second, network pharmacology and target validation were combined to identify the active ingredients, their targets, and associated pathways. Finally, MKN-45 and SNU-216 cell lines were used to explore the mechanisms by which noni juice inhibits cell proliferation, promotes lipid oxidation, and modifies mitochondrial morphology, thereby inducing ferroptosis *in vitro*. Results showed that noni juice significantly suppressed gastric cancer progression in mice. UPLC-Q Exactive MS analysis identified flavonoids—including apigenin, naringenin, and curcumol—as major blood metabolites. Both *in vivo* and *in vitro* experiments demonstrated that noni juice induced lipid peroxidation, leading to ferroptosis. Treatment with ferroptosis inhibitors successfully reversed this effect. Mechanistically, noni juice regulates the GPX4/HO-1 axis to induce ferroptosis. Pharmacological activation leads to the translocation of nuclear factor erythroid 2-related factor 2 (Nrf2) into the nucleus. This process increases the accumulation of lipid peroxidation and malondialdehyde induced by noni. Together, these data support that noni fruit juice suppresses gastric cancer progression and is associated with lipid peroxidation-driven ferroptotic injury involving the Nrf2/HO-1–GPX4 axis.

Received 17th August 2025,
Accepted 19th April 2026

DOI: 10.1039/d5fo03232f

rsc.li/food-function

Introduction

Gastric cancer (GC) poses a significant global health challenge, ranking as the fifth most common cancer worldwide and accounting for over 700 000 deaths in 2018.[1,2] While surgical resection remains the most effective treatment, targeted therapy and immunotherapy have shown notable progress. However, many patients are diagnosed at advanced stages, where therapeutic options remain limited.[3,4] Given the complexity of GC progression, inducing programmed cell death—including apoptosis, pyroptosis, and ferroptosis—has emerged as a critical strategy in GC treatment.[5] Thus, elucidating the signaling pathways associated with GC cell death and developing targeted therapies are urgent research priorities.

Dietary intervention is now considered a nontoxic, side-effect free anticancer strategy. Noni (*Morinda citrifolia* L.), a plant of the Rubiaceae family, thrives in Hainan's tropical climate and has been traditionally used in Chengmai—a renowned longevity town—for treating gastric ulcers, gastritis, *Helicobacter pylori* infections, and metabolic disorders.[6] Rich in bioactive compounds such as flavonoids, anthraquinones, polyphenols, and terpenoids, noni has shown broad medicinal properties.[7–9] For over 2000 years, noni juice, produced through natural fermentation, has served as both a functional food and a therapeutic agent, with a well-established safety profile. It is widely consumed as a health beverage for disease prevention and immune modulation.[10] Notably, noni exhibits potent anti-tumor effects against various cancers, including breast, lung, liver, and colorectal cancers.[11–13] Its anti-inflammatory, antioxidant, pro-apoptotic, and immunomodulatory properties further underscore its clinical value.[14]

Key Laboratory of Emergency and Trauma of Ministry of Education, Key Laboratory of Hainan Trauma and Disaster Rescue, Key Laboratory of Haikou Trauma, Engineering Research Center for Hainan Biological Sample Resources of Major Diseases, The First Affiliated Hospital of Hainan Medical University, Haikou 570102, PR China. E-mail: xiezhihao1008@163.com, luweifeng@hainmc.edu.cn, haoxinbao@tsinghua.org.cn, xulu2324@163.com

†These authors contributed equally to this paper and should be considered as co-first authors.

Mechanistically, alcohol-precipitated noni extracts enhance macrophage activity, stimulate nitric oxide synthesis, and upregulate tumor necrosis factors (TNFs), interferons (IFNs), and interleukins (ILs), thereby indirectly suppressing tumor growth and metastasis through immune activation.[15,16] Noni juice has been shown to inhibit the proliferation of Bel7402 liver cancer cells,[17] suppress MCF7 breast cancer cell growth and migration *via* mTOR pathway modulation,[14] and impede A549 lung cancer cell proliferation.[18] Additionally, it regulates glucose metabolism, lipid metabolism, inflammation, and oxidative stress.[19,20] Based on these findings, we hypothesized that noni juice may exhibit therapeutic potential against gastric cancer, prompting the current investigation.

Materials and methods

Antibodies and reagents

The following primary antibodies and reagents were used in this study: anti-Nrf2 (AF0639, Affinity Biosciences), anti-Keap1 (AF5266, Affinity Biosciences), anti-GPX4 (DF6701, Affinity Biosciences), anti-xCT (DF12509, Affinity Biosciences), anti-HO-1 (AF5393, Affinity Biosciences), lamin B1 rabbit polyclonal antibodies (EA041, ELK Biotechnology), anti-GAPDH rabbit pAb (GB11002, Servicebio), ferroptosis antibody sampler kit (#29650, Cell Signaling Technology), BDPY 581/591 C11 (S1068S, Beyotime), ferrous ion assay kit (S0043S, Beyotime), and ferrostatin-1 (HY-100579, MCE). Noni juice preparation: noni (*Morinda citrifolia* L.) fruits were harvested from Qiaotou, Chengmai County (Hainan Province, China), an area renowned for its longevity population. The traditional fermentation process was conducted by Hainan Fengxishu Noni Industry according to the following protocol: fresh fruits were washed and air-dried naturally. Whole fruits were fermented in sealed containers for 14 months. The fermented pulp was filtered through an 80-mesh sieve under sterile conditions. The juice was centrifuged at 4000*g* for 10 minutes. The final product underwent homogenization and sterilization.

Animal modeling and experimental design

All animal procedures were performed in compliance with the institutional guidelines and approved by the Animal Ethics Committee of Hainan Medical University (approval no. HYLL-2024-108). Animals and housing conditions: female C-NKG immunodeficient mice (n = 16) age: 7–8 weeks; weight: 20–25 g; housing: specific pathogen-free (SPF) facility; environmental conditions: temperature: 25 ± 1 °C, humidity: 50 ± 5% and light cycle: 12-hour light/dark. Orthotopic gastric cancer model establishment: cell preparation: SNU-216-luc human gastric cancer cells; cell suspension: 1×10^6 cells in 20 μL PBS/Matrigel (1 : 1) mixture; surgical procedure: cells injected into the gastric fundus serosal layer; post-operative monitoring for 3 days; experimental groups and treatment: grouping (days 6–9 post-implantation): treatment group (n = 8): noni juice (25 mL kg^{-1} day^{-1}, oral gavage) and control group (n = 8): PBS vehicle (25 mL kg^{-1} day^{-1}, oral gavage); treatment duration: 30 consecutive days of monitoring and analysis: bioluminescence imaging schedule: baseline: day 1; follow-up: days 10, 20, and 30; endpoint: euthanasia 72 hours post-final imaging and tissue collection for subsequent analysis.

Histopathological examination and immunohistochemical staining

Tissues were fixed in 4% paraformaldehyde for 24 hours and then transferred sequentially to 15 g per 100 mL and 30 g per 100 mL sucrose solutions for dehydration. Sections of 8 μm thickness were prepared using a cryostat. The sections were blocked with 5% bovine serum albumin for 30 minutes and incubated overnight at 4 °C with primary antibodies. Following incubation with fluorescently labeled secondary antibodies, the sections were visualized and analyzed using a fluorescence microscope.

Analysis and identification of secondary metabolites in noni juice

UPLC-Q Exactive MS technology was employed to identify the major secondary metabolites in noni juice following previously reported methods.[21–23] Further details are provided in the SI.

Network pharmacology analysis

Collection of *Morinda citrifolia* compounds and putative targets. Compositional identification revealed 45 components in *Morinda citrifolia* (HBJ). The 2D structures and SMILES structural formulae of these components were downloaded from the PubChem database (https://pubchem.ncbi.nlm.nih.gov/). Targets were collected from Swiss Target Prediction (https://www.swisstargetprediction.ch/) using a screening probability threshold of >0.

Screening of gastric cancer targets and ferroptosis targets. Genes related to GC were obtained from the GeneCards database (https://www.genecards.org/) using the search term "gastric cancer" and a gene score above the average. Ferroptosis-related targets were retrieved from the FerrDb database (https://www.zhounan.org/ferrdb/).

Construction of core targets. The intersection of compound putative targets and disease targets (OGEs) was mapped using the Gene Jvenn tool (https://jvenn.toulouse.inrae). All OGEs were imported into the STRING database (https://string-db.org/) to construct protein–protein interaction (PPI) networks. These networks were visualized using Cytoscape 3.7.2 software, and the CytoNCA plug-in was used to perform topological analyses to filter targets based on degree, closeness centrality (CC), and betweenness centrality (BC).

GO enrichment and KEGG pathway analysis. Functional enrichment analyses of GO categories (biological process [BP], molecular function [MF], and cellular component [CC]) and KEGG pathways were performed using the GENEDENOVO method. The filtering threshold for results was set at $p < 0.05$, and the counts were sorted in descending order.

Molecular docking. The 2D structural formulae of the compounds were downloaded from the PubChem database (https://pubchem.ncbi.nlm.nih.gov/). Protein structures of the

core proteins were retrieved from the PDB database (https://www.rcsb.org/). PDB format files with higher resolution and crystallographically complex proto-ligands were selected, and PyMol-2.5.2 software was used to remove water molecules and optimize receptor protein structures. AutoDockTools-1.5.7 software was employed for molecular docking, and the results were visualized using PyMol-2.5.2 software to construct interaction patterns.

Cell culture

Human poorly differentiated gastric adenocarcinoma cells (MKN45 and SNU216) were purchased from the Cell Bank of the Chinese Academy of Sciences, Shanghai, China. Cells were cultured in RPMI 1640 medium (C11875500BT, Gibco) supplemented with 10% fetal bovine serum (100270-106, Gibco) and 1% penicillin/streptomycin (BL505A, Biosharp) at 37 °C under a 5% CO_2 atmosphere. Cells were passaged every 2–3 days.

Cell viability and colony formation assay

Cell viability was assessed using Cell Counting Kit-8 (CCK-8) (Hanbio, Shanghai, China). A total of 3000 cells per well were seeded in a 96-well plate and treated with varying concentrations of noni for 24 or 48 hours. According to the manufacturer's protocol, 10 μL of CCK-8 reagent was added to each well, followed by incubation at 37 °C for 1 hour. Subsequently, absorbance at 450 nm was measured using an ELISA reader (Thermo Fisher Scientific), and the cell survival rate was calculated. For the colony formation assay, 500 cells were seeded into each well of a six-well plate, cultured for 24 hours, treated with noni for 48 hours, washed twice with PBS, and cultured for approximately two weeks. The cell cultures were fixed with 4% paraformaldehyde (Biosharp, Anhui, China) and stained with 0.1% crystal violet (G1014, Servicebio, Wuhan). Representative bacterial colonies were photographed and quantified.

Wound-healing and Transwell assays

Cells were seeded at a density of 6000 cells per well in a six-well plate. Upon reaching full confluence, a straight scratch was made using a 200 μL pipette tip, followed by washing with PBS. Cells were treated with varying concentrations of noni, and the wound area (BZ-X800LE, Keyence) was photographed at 0, 24, and 48 hours. Dashed lines were used to delineate the wound boundaries, and the wound healing rate was quantified using ImageJ software. For the Transwell assay, Matrigel (R&D, USA) was diluted (1 : 1), and 100 μL was added to the upper chamber of each Transwell insert and allowed to solidify in an incubator for 2–3 hours. For migration experiments, this step was omitted. A cell suspension (200 μL per well) containing approximately 3000–5000 cells was added to the upper chamber, while 20% FBS cell culture medium and varying concentrations of noni were added to the lower chamber. After 24 hours of incubation at 37 °C under a 5% CO_2 atmosphere, cells were fixed with 4% paraformaldehyde and stained with 0.5% crystal violet. Images were captured using an inverted microscope (Olympus IX73, Japan), and cell numbers were analyzed.

Cell apoptosis and cell cycle analyses by flow cytometry

Apoptosis of gastric cancer cells was assessed *via* flow cytometry. Cells were incubated with noni for 48 hours, followed by double staining with annexin V-FITC and PI, and subsequently analyzed using a flow cytometer. Additionally, cell cycle arrest was analyzed *via* flow cytometry. Data visualization and statistical analyses were performed using GraphPad Prism (version 8, GraphPad Software), employing two-tailed *t*-tests.

RNA-Seq

RNA-Seq was conducted as previously described by Cai *et al.*[24] Detailed procedures are provided in the SI.

Detection of lipid peroxidation levels and glutathione assays

The levels of GSH and MDA in cell or tissue lysates were determined according to the manufacturer's instructions. Details are provided in the SI.

Western blot analyses

Western blotting (WB) was performed as previously described by Cai *et al.*[24] Detailed procedures are included in the SI.

Mitochondrial membrane potential measurement

The mitochondrial membrane potential was evaluated using a JC-1 probe (Beyotime). Cells were labeled with JC-1 staining dye at 37 °C for 20 minutes, washed twice to remove residual fluorescent probes, and examined using a laser-scanning confocal microscope (Zeiss).

Measurement of reactive oxygen species (ROS)

ROS levels in gastric cancer cells were measured using the DCFH-DA fluorescent probe. Cells were treated with noni for 48 hours and stained with the DCFH-DA probe according to the commercial kit instructions. Fluorescence signals were captured and analyzed using a fluorescence microscope or flow cytometry.

Transmission electron microscopy (TEM)

TEM was conducted as previously described by Chen *et al.*[25] Details are provided in the SI.

Immunofluorescence staining

During immunofluorescence staining, the treated cells were fixed in 4% formaldehyde and then permeabilized with 0.1% Triton X-100. After removing the permeabilization solution by washing, the cells were blocked with 5% goat serum for 1 hour at room temperature. Subsequently, incubation was carried out with GPX4 (DF6701, Affinity Biosciences) antibodies at 4 °C for 12–16 hours. The cells were washed five times for 5 minutes each at room temperature in PBST, followed by incubation with YS Fluor™ 594 goat anti-rabbit antibodies (33112ES60, Yeasen) for 2 hours at 37 °C. The dish was washed five times for 5 minutes at room temperature in PBST and then incubated with 4′,6-diamidino-2-phenylindole (DAPI) for 10 minutes. Following the final staining and washing steps,

images were acquired using a microscope. The EdU assay, ferrous ion assay, and C11-BODIPY 581/591 staining were performed following the manufacturer's instructions (Beyotime).

Statistical analysis

All results are expressed as mean ± SD. Statistical analyses were conducted using two-tailed unpaired *t*-tests and one-way analysis of variance (ANOVA) using GraphPad Prism software. Differences with *p*-values <0.05 were considered statistically significant.

Results

Effect of noni juice on histopathological changes in gastric cancer

An *in situ* gastric cancer model was successfully established through the cultivation of gastric cancer cells and subsequent treatment studies in C-NKG mice. Each C-NKG mouse was injected with 20 μL of a cell suspension containing 1×10^6 cells (suspended in PBS and Matrigel) into the serosal layer of the gastric fundus. Fluorescence values were monitored on the third postoperative day. *In vivo* imaging confirmed the successful establishment of the *in situ* gastric cancer model in C-NKG mice. Based on fluorescence intensity, mice were randomly assigned to two groups: a control group, which received daily gavage with PBS, and a treatment group, which received daily gavage with 25 mL kg^{-1} noni juice, as illustrated in Fig. 1A.

As shown in Fig. 1B, noni juice did not suppress tumor growth by day 10; however, by day 20, imaging data indicated that noni juice significantly inhibited the growth of gastric cancer cells, evidenced by a marked reduction in the region of interest (ROI) values. By day 30, the ROI values in the treatment group exhibited an even greater reduction compared to the control group. Fig. 1C and D show the stomach weight of the control group and the noni treatment group. Fig. 1E presents the anatomical diagram. Weight analysis revealed that weight gain in the later stages of the study was attributable to the accumulation of abdominal fluid. Anatomical analysis of the gastric tissue demonstrated that gastric cancer progression was significantly reduced in the treatment group compared with the control group. These findings indicate that active compounds in noni juice effectively inhibit tumor growth in gastric cancer.

Analysis revealed that after noni treatment, the pathological changes in the stomach were alleviated and the overall tumor size decreased. Histopathological examination using H&E staining revealed distinct differences between the groups. As shown in Fig. 1F, the H&E-stained sections of gastric cancer tissue from control mice treated with PBS exhibited infiltrative growth of cancer cells, often as single entities, accompanied by the proliferation of surrounding fibrous tissue. Conversely, in mice treated with noni juice for 30 days, gastric cancer tissue displayed significant differentiation, with evidence of coagulative necrosis. These findings suggest that noni juice induces necrosis in gastric cancer tissue.

Blood component analysis

Using UPLC-Q Exactive MS, a total of 362 components were identified in the traditional Chinese medicine formula. Among these, 45 were prototype blood components. Table 1 summarizes the retention time (RT), predicted chemical formulae, average mass-to-charge ratios, ion modes, and identification scores of the detected ion components. The most abundant component classifications were carboxylic acids and derivatives (13.81%), fatty acyls (13.33%), prenol lipids (11.43%), and organooxygen compounds (10%). The positive and negative ion spectra of the serum containing the formula are shown in Fig. 2A.

Previous studies have reported that these compounds exert cytotoxic effects on tumor cells, potentially contributing to the antitumor activity of noni juice.[26] A detailed analysis of the primary blood components of noni juice, as summarized in Table 1, identified flavonoids such as apigenin 7-*O*-glucuronide, genistein, naringenin-7-*O*-beta-D-glucuronide, and curcumol as key contributors to tumor inhibition.

The content of the active component apigenin 7-*O*-glucuronide was quantified using a Waters Acquity UPLC I-Class ultra-performance liquid chromatograph. The total ion chromatogram (TIC) of the standard solution, the standard curve of apigenin 7-*O*-glucuronide, and the TIC of the sample are presented in Fig. 2B–D. Using TargetLynx quantitative software with a retention time error tolerance of 15 seconds, the concentration of apigenin 7-*O*-glucuronide in noni juice was calculated as 0.9643 ng mL^{-1}.

Literature analysis reveals that apigenin 7-*O*-glucuronide possesses anti-inflammatory, antioxidant, and anticancer properties. Previous studies have demonstrated that this compound inhibits HeLa cell proliferation by inducing apoptosis, arresting the cell cycle at the G0/G1 phase, reducing mitochondrial membrane potential (MMP), and increasing intracellular ROS production. This cascade leads to mitochondrial dysfunction and triggers ferroptosis.[27–31] These findings support the validation of the antitumor effects of noni juice from the perspective of ferroptosis.

Network pharmacology analysis and validation

Based on the analysis of blood component metabolic products, combined with GC-related genes obtained from the GeneCards database (https://www.genecards.org/), genes with scores above the average threshold for gastric cancer were selected. Ferroptosis-related targets were filtered from the FerrDb database (https://www.zhounan.org/ferrdb/), resulting in the identification of 71 target genes associated with GC (Fig. 3A). Eleven core targets with potential therapeutic relevance for gastric cancer through ferroptosis were identified, as shown in Fig. 3B.

These eleven core targets were imported into the DENOVO tool for GO enrichment and KEGG pathway analysis. The GO enrichment analysis identified a total of 3038 items, of which 2458 were statistically significant. Specifically, GO-Biological Process (GO-BP) enrichment analysis yielded 2636 items, with

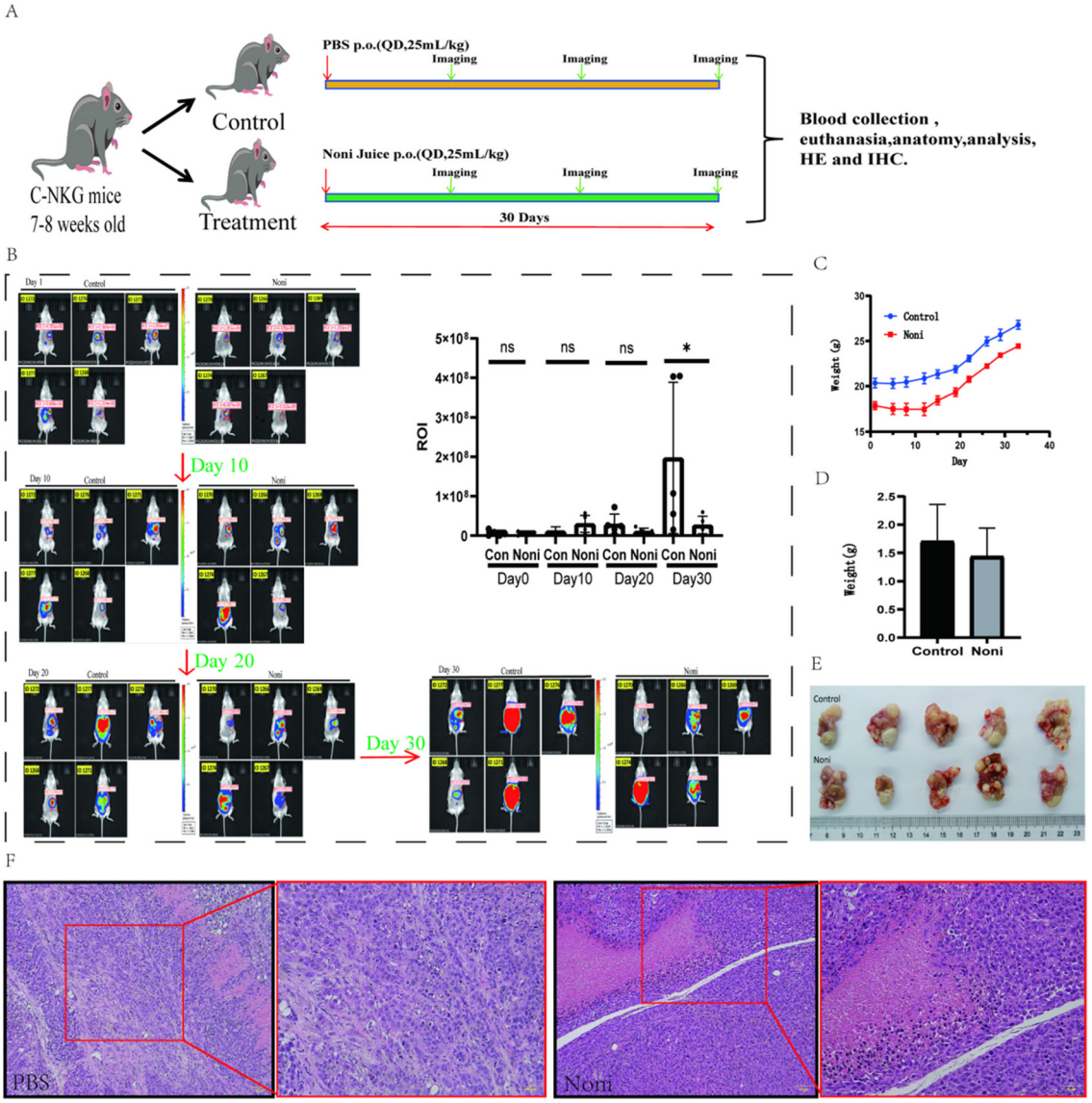

Fig. 1 Antitumor effects of noni juice on mice. The model group (administered daily with PBS) and the noni group (administered daily with 25 mL kg^{-1} noni juice) were compared. (A) Schematic of the experimental design and timeline. (B) Bioluminescence imaging of mice *in vivo* (n = 5), showing tumor luciferase signals at days 0, 10, 20, and 30. (C) Weight analysis of GC xenograft mice in each group. (D) Tumor weight analysis in GC xenograft mice. (E) Representative images of xenograft tumors after treatment with noni juice. (F) H&E-stained sections of tumor tissue from each group. Scale bar is 50 μm. Data are presented as mean ± SD. Statistical significance is indicated as follows: *p < 0.05 and **p < 0.01 compared to the control group.

2201 being statistically significant; GO-Molecular Function (GO-MF) analysis identified 218 items, with 171 being statistically significant; and GO-Cellular Component (GO-CC) analysis revealed 184 items, with 86 being statistically significant. The KEGG enrichment analysis identified 179 signaling pathways associated with the eleven core targets. Applying a significance threshold of $P < 0.05$, 132 pathways were selected, with the top 20 presented in a bubble chart. After excluding pathways related to diseases, three key signaling pathways were identified: the HIF-1 signaling pathway, the C-type lectin receptor signaling pathway, and the thyroid hormone signaling pathway. These three pathways are predicted to be central mechanisms for HBJ's therapeutic effects on GC.

To elucidate the interactions among HBJ, ferroptosis, and GC, a key herbal medicine–compound–target–pathway interaction network was constructed. Using Cytoscape 3.7.2, the top three signaling pathways with the smallest *P*-values and their corresponding targets were visualized, resulting in a network graph comprising 39 nodes and 116 edges. A Sankey diagram was also constructed, representing hub genes associated with the three core signaling pathways and relatively active compounds (Fig. 3C and D).

Table 1 Summary of prototype main blood entering components

Serial number	Metabolite	Retention time (min)	Mode	Adducts	Formula	*m/z*	Fragmentation score
1	Apigenin 7-*O*-glucuronide	6.00	Pos	M + H	$C_{21}H_{18}O_{11}$	447.09	97.20
2	Cholic acid	9.12	Pos	M + H-2H_2O, M + NH_4, M + Na, M + H-H_2O, 2M + H	$C_{24}H_{40}O_5$	373.27	94.40
3	Wogonoside	5.42	Pos	M + H	$C_{22}H_{20}O_{11}$	461.11	92.80
4	Genistein	7.88	Pos	M + H	$C_{15}H_{10}O_5$	271.06	92.30
5	Enniatin B	13.79	Pos	M + NH_4	$C_{33}H_{57}N_3O_9$	657.44	90.50
6	Thunberginol C	7.69	Pos	M + H	$C_{15}H_{12}O_5$	273.08	78.60
7	*sec*-*O*-Glucosylhamaudol	6.22	Neg	M-H_2O-H	$C_{21}H_{26}O_{10}$	419.13	78.50
8	3-Hydroxy-12-oxochol-9(11)-en-24-oic acid	8.50	Pos	M + H-2H_2O, M + H-H_2O, M + H	$C_{24}H_{36}O_4$	353.25	78.20
9	Ginkgolic acid C17:2	7.57	Pos	M + H-2H_2O, M + H, M + H-H_2O	$C_{24}H_{36}O_3$	337.25	77.50
10	Vicine	0.80	Neg	M-H_2O-H, M + Na-2H	$C_{10}H_{16}N_4O_7$	325.08	76.30
11	Curcumenol	12.15	Pos	M + H	$C_{15}H_{22}O_2$	235.17	75.40
12	Ketolithocholic acid	8.34	Pos	M + H-H_2O	$C_{24}H_{38}O_4$	373.27	74.00
13	Hydroxyisolathyrol	8.47	Pos	M + H-H_2O	$C_{20}H_{30}O_5$	333.21	73.80
14	Hydrangenol 8-*O*-glucoside	6.35	Pos	M + H, M + NH_4, M + H-2H_2O	$C_{21}H_{22}O_9$	436.16	73.40
15	Naringenin-7-*O*-beta-D-glucuronide	5.72	Pos	M + H-H_2O	$C_{21}H_{20}O_{11}$	431.10	72.60
16	Lactucin	8.66	Pos	M + H-H_2O	$C_{15}H_{16}O_5$	259.10	71.90
17	Deoxy-11-oxoandrographolide	10.47	Pos	M + NH_4	$C_{20}H_{28}O_5$	366.23	68.90
18	Pterisolic acid F	8.25	Pos	M + H-2H_2O	$C_{20}H_{30}O_6$	331.19	68.80
19	Curcumol	11.84	Pos	M + H	$C_{15}H_{24}O_2$	237.19	68.50
20	Neoruscogenin	10.18	Pos	M + ACN + Na	$C_{27}H_{40}O_4$	492.31	67.70
21	Isosteviol	10.95	Pos	M + H	$C_{20}H_{30}O_3$	319.23	67.20
22	Gingerol	10.01	Pos	M + H	$C_{21}H_{34}O_4$	351.25	66.80
23	Triptotin F	9.37	Pos	M + ACN + Na	$C_{31}H_{44}O_5$	560.33	66.50
24	*O*-Acetylisocalamendiol	10.50	Pos	M + H-H_2O	$C_{17}H_{28}O_3$	263.20	65.90
25	3,14,20-Trihydroxypregn-5-en-15-one	7.35	Pos	M + H	$C_{21}H_{32}O_4$	349.24	62.00
26	Albatrelin G	11.71	Pos	M + 2Na-H	$C_{22}H_{32}O_3$	389.21	61.70
27	Sambunigrin	1.61	Neg	M + FA-H	$C_{14}H_{17}NO_6$	340.10	61.60
28	Periplocoside N	8.85	Pos	M + H-2H_2O	$C_{27}H_{44}O_6$	429.30	61.40
29	Indolepropionic acid	7.48	Pos	M + H, 2M + H	$C_{11}H_{10}NO_2$	189.08	60.40
30	Longifloroside A	5.34	Neg	M-H_2O-H	$C_{27}H_{34}O_{11}$	515.19	59.90
31	6alpha-Hydroxynidorellol	12.39	Pos	M + H-H_2O	$C_{20}H_{34}O_3$	305.25	59.20
32	Sarcostin	7.15	Pos	M + H-2H_2O	$C_{21}H_{34}O_6$	347.22	58.90
33	Salaspermic acid	12.12	Pos	M + ACN + Na	$C_{30}H_{48}O_4$	536.37	57.10
34	Siraitic acid B	9.02	Pos	M + ACN + H	$C_{29}H_{42}O_5$	512.33	55.90
35	Digoxigenin	7.80	Pos	M + CH_3OH + H	$C_{23}H_{34}O_5$	423.27	54.70
36	8alpha-Hydroxylabda-13(16),14-dien-19-yl *p*-hydroxycinnamate	9.81	Pos	M + ACN + H	$C_{29}H_{40}O_4$	494.32	54.00
37	Cortodoxone	8.22	Pos	M + H-H_2O, M + H	$C_{21}H_{30}O_4$	347.22	53.40
38	*N*-Acetyl-L-tyrosine	6.11	Pos	M + H-2H_2O	$C_{11}H_{13}NO_4$	188.07	52.50
39	Acetylintermedine	9.05	Pos	M + NH_4	$C_{17}H_{27}NO_6$	359.22	52.40
40	Germacrone 4,5-epoxide	10.37	Pos	M + H-H_2O	$C_{15}H_{22}O_2$	217.16	52.30
41	*N*-Acetyl-phenylalanine	5.93	Neg	M + FA-H	$C_{11}H_{13}NO_3$	252.09	51.90
42	Desferrioxamine H	1.35	Pos	M + 2Na-H	$C_{20}H_{36}N_4O_8$	505.23	51.60
43	Estrone sulfate	8.02	Pos	M + 2Na-H	$C_{18}H_{22}O_2$	315.13	51.50
44	18-Nor-4,15-dihydroxyabieta-8,11,13-trien-7-one	6.78	Pos	M + CH_3OH + H	$C_{19}H_{26}O_3$	335.22	51.10
45	Melliferone	11.48	Pos	M + ACN + H	$C_{30}H_{44}O_4$	510.36	50.40

The active ingredients of noni juice—apigenin 7-*O*-glucuronide, genistein, naringenin-7-*O*-beta-D-glucuronide, and curcumol—were evaluated for their binding energy with the core proteins EGFR and MAPK3 (Fig. 3F). Among these, apigenin 7-*O*-glucuronide and naringenin-7-*O*-beta-D-glucuronide exhibited stable binding. Analysis revealed that the HIF-1 signaling pathway influences ferroptosis. To validate the reliability of the network pharmacology findings, noni-treated cells were analyzed using western blotting (Fig. 3E). The results showed that the active ingredients of noni juice affect key targets, including STAT3 and HIF1α. Expression levels of STAT3 and HIF1α decreased following treatment with noni juice, but partially rebounded upon the addition of Fer-1. HIF1α expression was reduced, thereby inhibiting glycolysis. The STAT3/HIF-1α signaling pathway was shown to inhibit energy metabolism and the secretion of inflammatory factors in gastric cancer cells, resulting in irreversible oxidative stress and the induction of ferroptosis.

Effect of noni juice on the activity of gastric cancer cells

Cellular functional experiments using noni juice were conducted, and the results are presented in Fig. 4. As shown in Fig. 4A, a CCK-8 assay was used to evaluate the effect of noni juice at different concentrations. When MKN45 gastric cancer cells were treated with 15% noni juice for 24 hours, cell viability was reduced to 53.99%, while SNU216 cells exhibited a via-

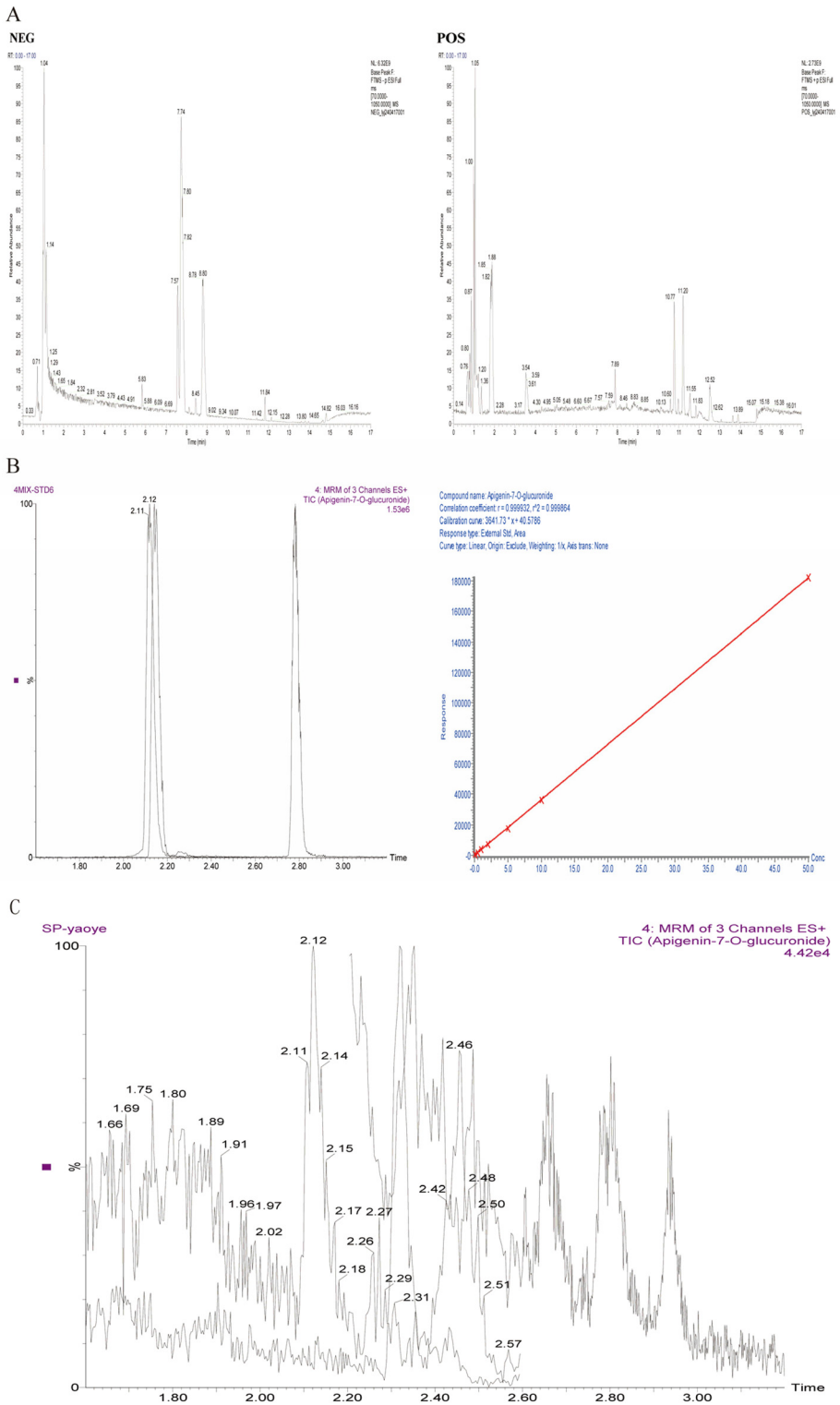

Fig. 2 Identification of serum metabolic components using UPLC-Q Exactive MS. (A) The serum metabolic components identified using UPLC-Q Exactive MS in both positive and negative ion modes. (B) The total ion chromatogram (TIC) of the standard solution along with the corresponding standard curve. (C) The TIC of noni juice.

bility of 61.91%. After 48 hours of treatment with 15% noni juice, cell viability decreased further, reaching 28.41% for MKN45 cells and 49.3% for SNU216 cells. A dose-dependent reduction in cell viability was observed up to a concentration of 20% noni juice, beyond which the cells became nearly completely inactive.

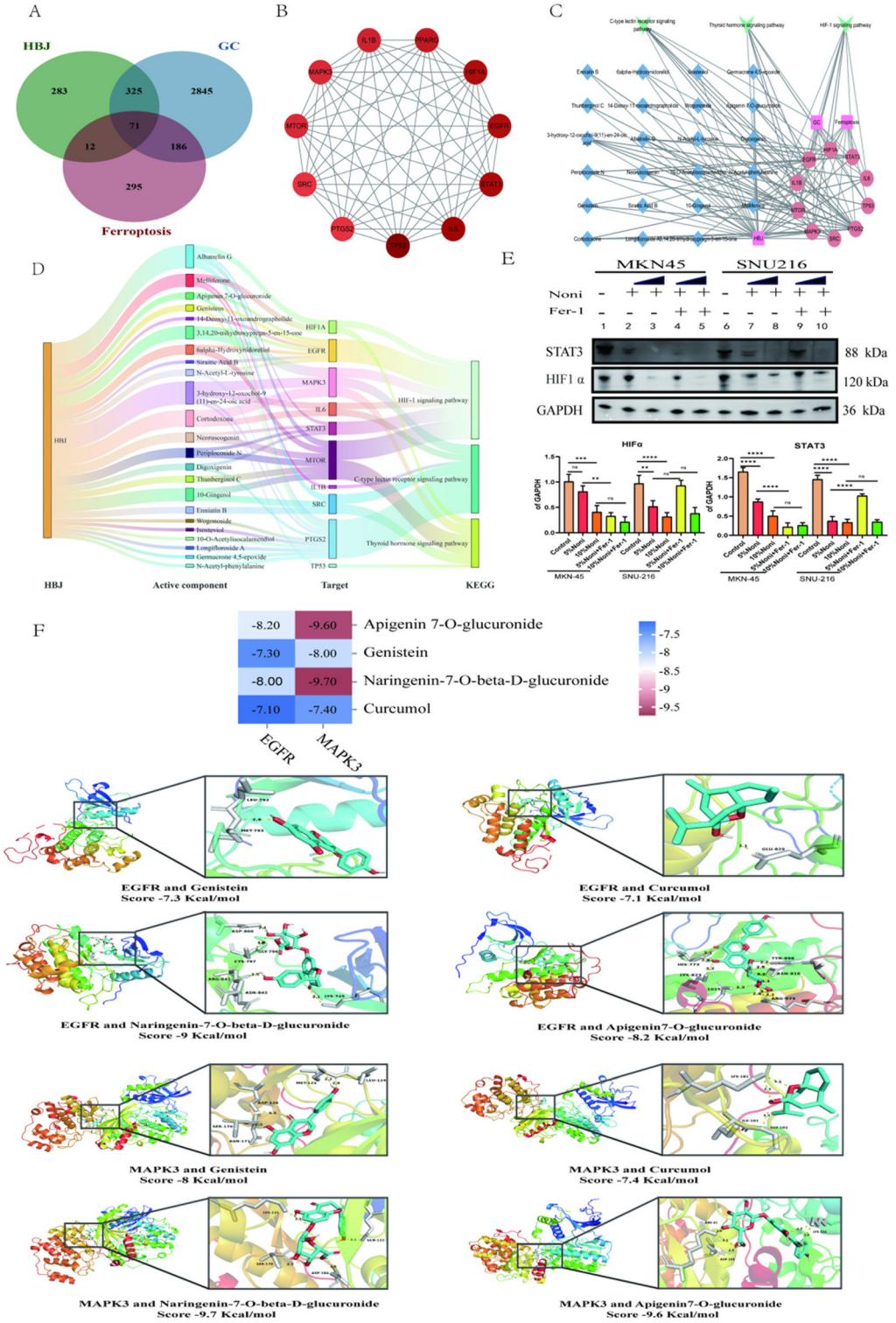

Fig. 3 Network pharmacological analysis for identifying predominant anti-GC compounds in noni juice. (A) Overlap analysis of noni juice targets, GC-related genes, and ferroptosis-associated targets. (B) Screening of core target genes. (C and D) Key compound–target–pathway network of noni juice in GC treatment. (E) Validation of key targets in network pharmacology using western blotting. (F) Molecular docking of major metabolites in noni juice. Data are presented as mean ± SD. Statistical significance is indicated as follows: *$p < 0.05$, **$p < 0.01$, ***$p < 0.001$ and ****$p < 0.0001$ compared to the control group.

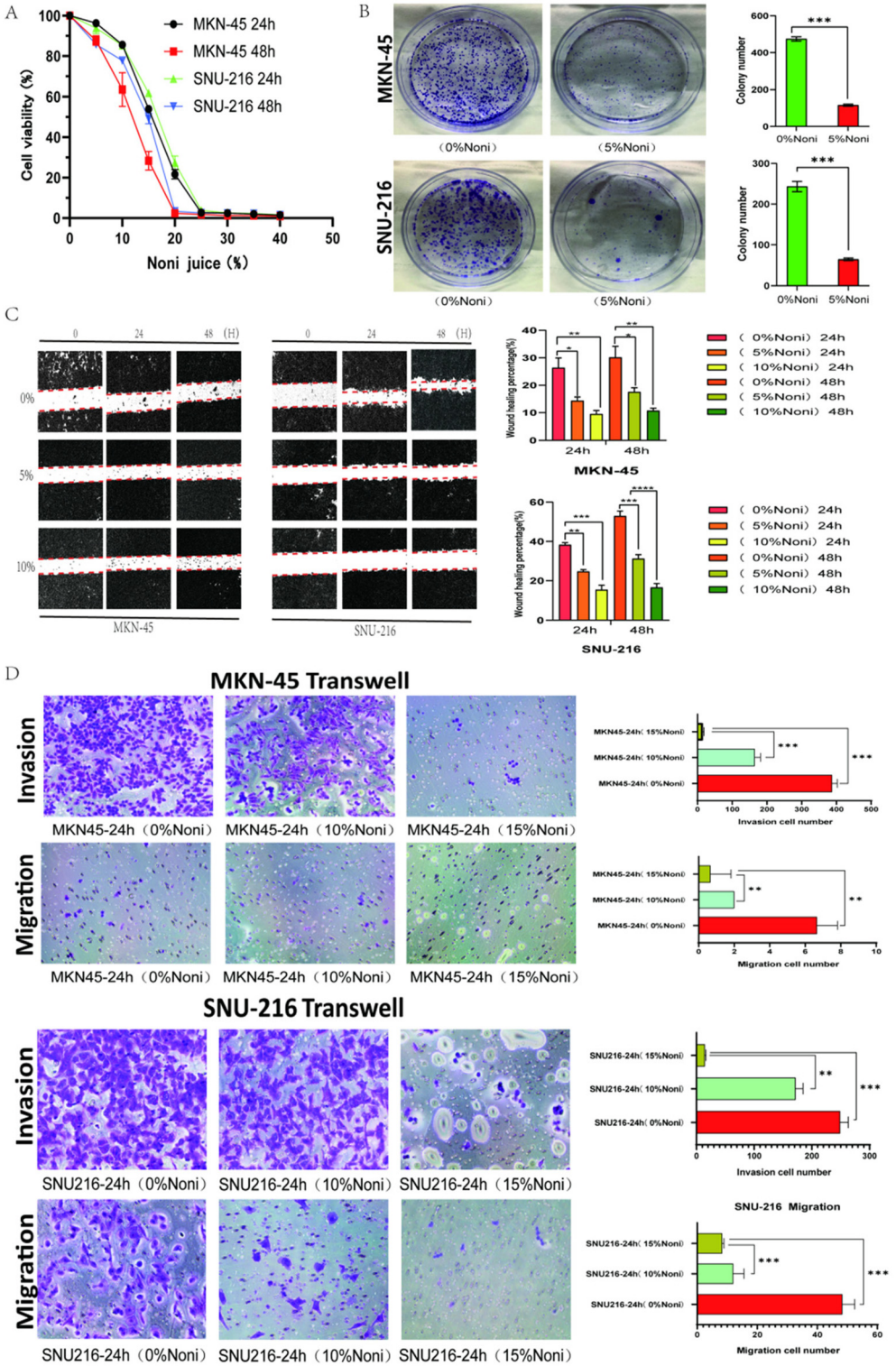

Fig. 4 Noni juice induces cell death and inhibits proliferation in gastric cancer cells. (A) Cell viability was measured using CCK-8 assays. (B) Colony-formation assays were performed on MKN-45 and SNU-216 cells, with colony numbers quantified using ImageJ software. (C) Wound-healing assays were conducted to evaluate the migratory capacity of MKN-45 and SNU-216 cells following treatment with noni juice. Scale bars represent 200 μm. (D) Transwell assays were used to assess the invasion and migration abilities of MKN-45 and SNU-216 cells after noni juice treatment. Scale bars represent 50 μm. Data are presented as mean ± SD. Statistical significance is indicated as follows: *$p < 0.05$, **$p < 0.01$, ***$p < 0.001$ and ****$p < 0.0001$ compared to the control group.

A clonogenic assay (Fig. 4B) revealed a progressive decline in the number of cell colonies with increasing concentrations of noni juice. At a concentration of 10%, no significant clonal growth was observed, confirming the ability of noni juice to inhibit gastric cancer cell proliferation at low doses.

The scratch assay (Fig. 4C) was employed to evaluate the effect of noni juice on wound healing in gastric cancer cells. Results indicated that the intervention significantly impaired scratch closure, suggesting that noni juice inhibited both the repair of scratch-induced injury and the migration of gastric cancer cells.

Additionally, the Transwell assay (Fig. 4D) demonstrated that the migratory and invasive abilities of MKN45 and SNU216 cells were markedly reduced in a concentration-dependent manner with increasing amounts of noni juice. These results were statistically significant, indicating the potent inhibitory effect of noni juice on the migration and invasion of gastric cancer cells.

Effects of noni juice on apoptosis, cell cycle, and the transcriptome of gastric cancer cells

SNU-216 cells were treated with 0% noni juice (control group) and 15% noni juice (treatment group) for 48 hours. The apoptosis of cells in both groups was analyzed using annexin FITC and PI dual staining, as shown in Fig. 5A. The 15% noni treatment group exhibited a statistically significant increase in apoptosis compared to the PBS control group.

The effects of noni juice on the cell cycle of SNU-216 cells were evaluated using the PI staining method and flow cytometry. As shown in Fig. 5B, significant changes were observed in the G0/G1 and S phases of the cell cycle between the 15% noni treatment group and the PBS control group. Specifically, the proportion of cells in the G0/G1 phase decreased by 25.66%, while the proportion of cells in the S phase increased by 76.57%. These results indicate that noni juice reduces the number of G0/G1 phase cells, increases S phase cells, disrupts DNA synthesis, and promotes cell death.

To further investigate the effects of noni juice on gastric cancer cells, transcriptome sequencing was performed on SNU-216 cells after treatment with it. The experiments were repeated in triplicate. The results are shown in Fig. 5C; specifically, Fig. 5C1 presents the clustering heatmap of the transcriptome analysis. RNA-seq analysis identified significant changes in gene expression, with 634 genes upregulated and 550 genes downregulated. Among these, ferroptosis-related genes, including *SAT1*, *HMOX1*, *SAT2*, and *MAP1LC3B2*, were upregulated. Fig. 5C2 shows the volcano plot of differential gene expression, highlighting *HSPA6* as the most significantly upregulated gene. HSPA6, a heat shock protein, mediates cellular stress responses, induces protein misfolding, and promotes the expression of molecular chaperones that regulate lysosomal autophagy and mitochondrial ATP functions.

GO enrichment analysis is presented in Fig. 5C3 and C4. Fig. 5C3 reveals downregulation in biological processes associated with calcium ion regulation, respiratory chain components, and transmembrane protein functions. In contrast, Fig. 5C4 shows upregulation in biological processes linked to cellular adaptive response signaling, nucleosome organization, DNA packaging complexes, protein–DNA complexes, and molecular functions related to protein folding chaperones.

KEGG pathway enrichment analysis (Fig. 5C5 and C6) indicates a significant downregulation of the oxidative phosphorylation signaling pathway and an upregulation of the MAPK signaling pathway. These pathways are associated with cell proliferation and metastasis. The oxidative phosphorylation pathway, as a critical site for mitochondrial energy exchange, influences cellular metabolism, tumorigenesis, and tumor progression.

These RNA-seq findings provide a foundation for subsequent experiments. Based on the results, it is inferred that the active components of noni juice may activate ferroptosis in gastric cancer cells.

Noni Juice activates ferroptosis in gastric cancer research

SNU-216 and MKN-45 cells were treated with noni juice for 48 hours, while PBS-treated cells served as the control group. The intracellular levels of glutathione (GSH) and malondialdehyde (MDA) were analyzed. As shown in Fig. 6A, the GSH content decreased significantly, while the MDA content increased following noni juice treatment. Reactive oxygen species (ROS) production was assessed using the fluorescent probe DCFH-DA, and the results, depicted in Fig. 6B, showed a significant increase in ROS levels in the noni-treated group compared to the control group.

The mitochondrial membrane potential (MMP) was evaluated using the fluorescent probe JC-1. As shown in Fig. 6C, cells treated with noni juice exhibited a significant increase in mitochondrial membrane potential compared to the control group, indicating altered mitochondrial function. Western blot (WB) analysis was employed to study the expression of ferroptosis-related proteins. As shown in Fig. 6D, noni juice treatment upregulated the expression of heme oxygenase-1 (HO-1), leading to a significant accumulation of MDA and a reduction in glutathione peroxidase 4 (GPX4) levels.

Further analysis of the expression of Kelch-like ECH-associated protein 1 (Keap1), nuclear factor erythroid 2-related factor 2 (Nrf2), and GPX4 proteins revealed that noni juice disrupted the Keap1–Nrf2 complex in gastric cancer cells. This disruption resulted in the degradation of Keap1 and the nuclear translocation of Nrf2. Increased HO-1 expression and decreased GPX4 levels led to the accumulation of nuclear Nrf2, which inhibited cystine import, reduced GSH synthesis, and promoted the accumulation of lipid hydroperoxides (PLOOHs). These processes caused irreversible damage to cell membranes and induced ferroptosis.

The system Xc–GSH–GPX4 pathway, a critical cellular defense mechanism against ferroptosis, was disrupted due to the inhibition of cystine transport by the Xc-system. This collapse of ferroptosis defense mechanisms led to excessive lipid peroxidation on the cell membrane and ultimately ferroptosis. The Xct–4F2hc complex has been identified as a potential therapeutic target for anticancer drug development. Additionally, noni juice treatment decreased the expression of nuclear receptor coactivator 4 (NcoA4) and increased the

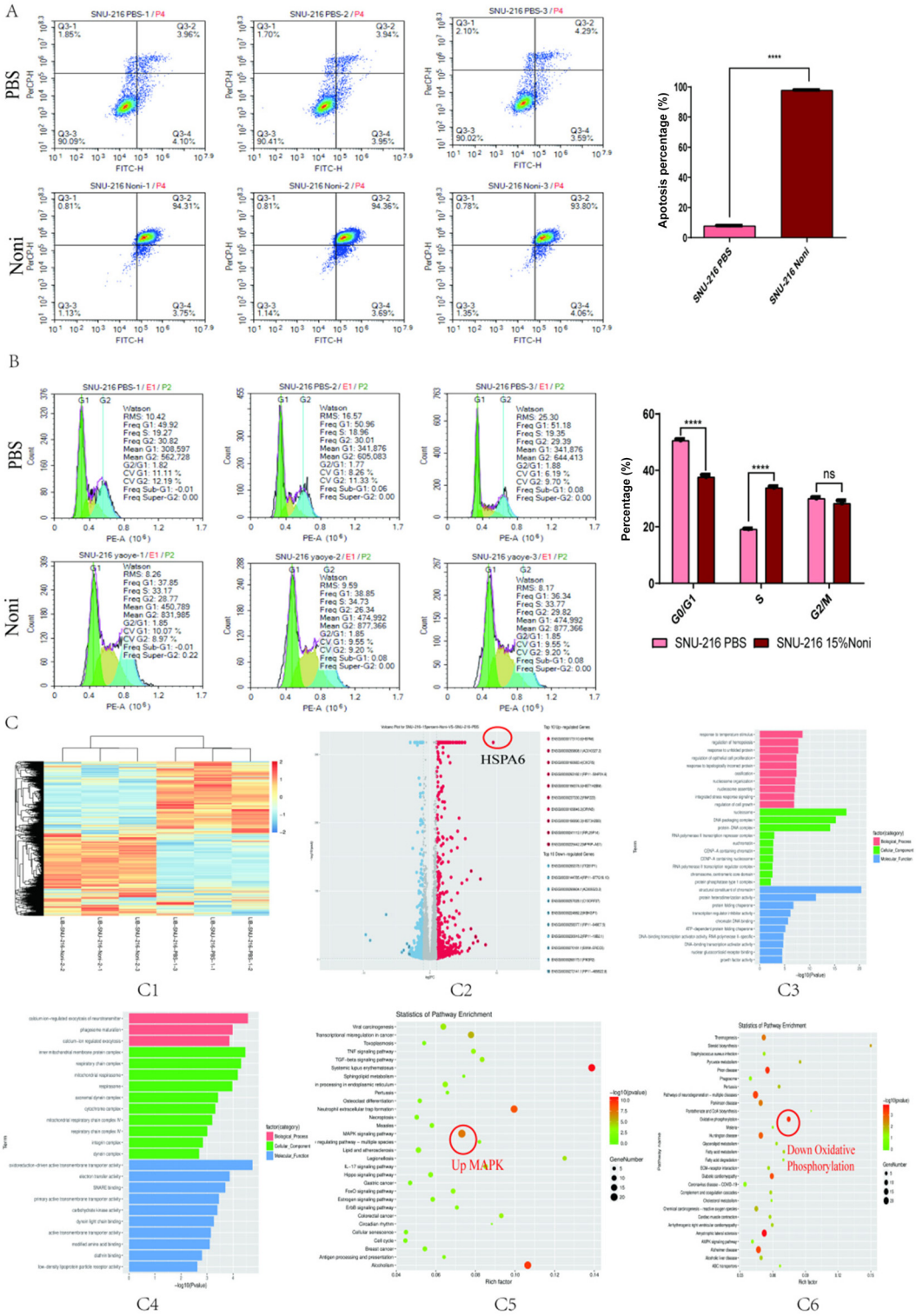

Fig. 5 Effects of noni juice on apoptosis and the cell cycle in SNU-216 cells. (A) Apoptotic analysis of SNU-216 cells treated with noni juice. (B) Effects of noni juice on the cell cycle of SNU-216 cells. (C1) Gene clustering heatmap. (C2) Volcano plot of differentially expressed genes. (C3 and C4) GO enrichment analysis of differentially expressed genes. (C5 and C6) KEGG pathway enrichment analysis of differentially expressed genes. Data are presented as mean ± SD. Statistical significance is indicated as follows: *$p < 0.05$, **$p < 0.01$, ***$p < 0.001$ and ****$p < 0.0001$ compared to the control group.

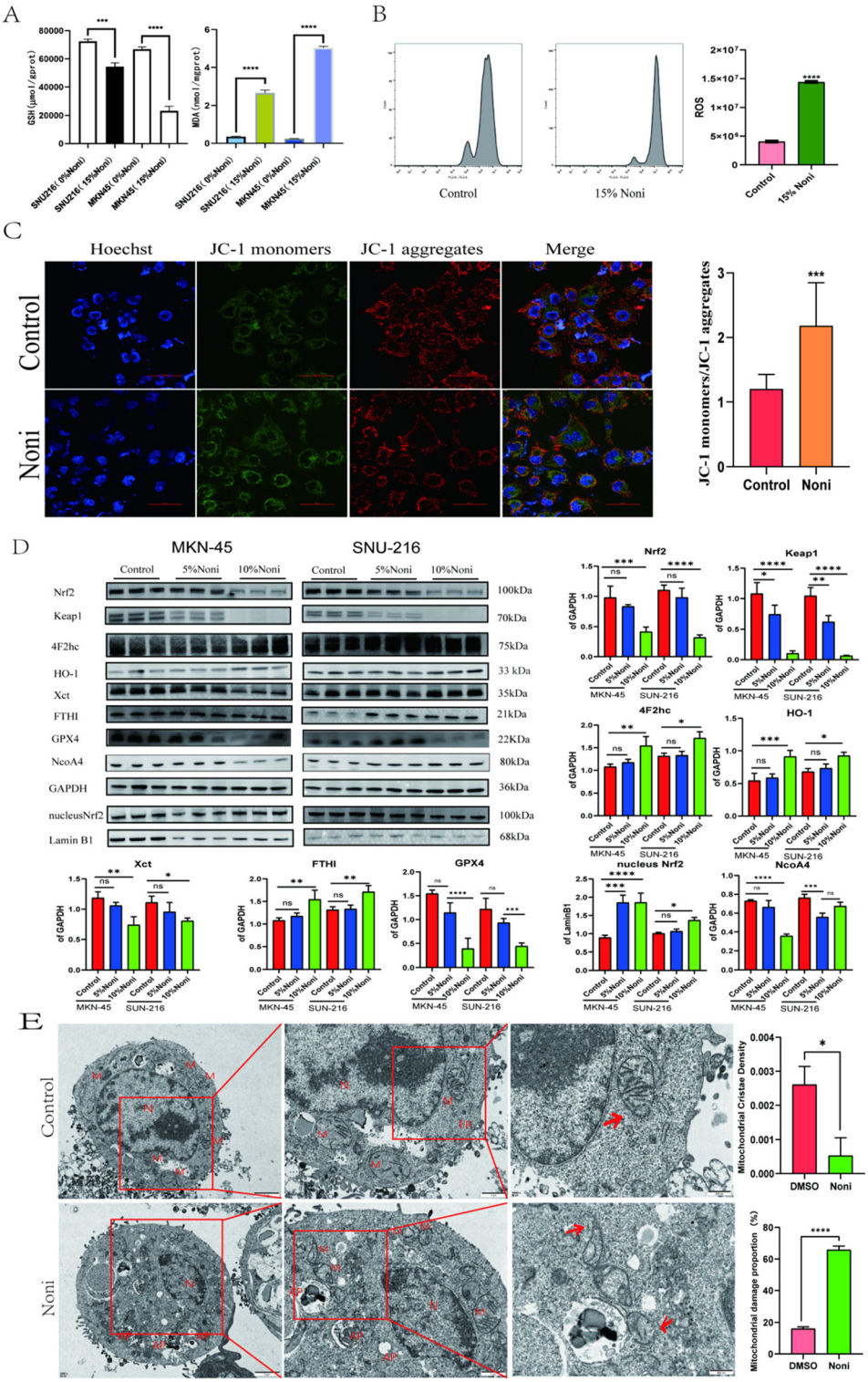

Fig. 6 Effects of noni juice on ROS, MMP, mitochondria, and the regulation of key proteins in the Nrf2/HO-1 pathway in gastric cancer cells. (A) MDA and GSH levels in gastric cancer cells after incubation with noni juice for 48 hours. (B) ROS levels in SNU-216 cells measured using the DCFH-DA fluorescent probe. (C) MMP levels detected by JC-1 staining after 48 hours of noni juice treatment. (D) Effects of noni juice on the expression of Nrf2/HO-1 proteins in gastric cancer cells. (E) Mitochondrial morphology in SNU-216 cells before and after noni juice treatment observed *via* transmission electron microscopy. Data are presented as mean ± SD. Statistical significance is indicated as follows: *$p < 0.05$, **$p < 0.01$, ***$p < 0.001$ and ****$p < 0.0001$ compared to the control group.

expression of ferritin heavy chain 1 (FTH1), thereby affecting lysosomal autophagy.

Transmission electron microscopy (TEM) was used to observe SNU-216 cells before and after noni juice treatment, as shown in Fig. 6E. In the control group, cells exhibited regular morphology, with nuclei (N) having an irregular oval shape, distinct nucleoli, and short rod- or oval-shaped mitochondria (M) with clear inner cristae and intact structures. The endoplasmic reticulum (ER) structure was also well-defined. In contrast, cells in the noni-treated group displayed an irregular morphology, including irregularly shaped nuclei (N), reduced nucleoli, and perinuclear condensation of heterochromatin. Most mitochondria (M) were oval, with slightly blurred cristae, and some mitochondria were abnormally shaped. The ER structure remained clear, and numerous autophagosomes (AP) were observed in the cytoplasm. A blind semiquantitative analysis method was used to conduct the quantification of transmission electron microscopy (TEM) images. The results showed that after noni treatment, the crista density of gastric cancer cell mitochondria decreased, the number of damaged mitochondria increased, and the mitochondria exhibited characteristics of ferroptosis. Biochemical markers included ROS accumulation, extensive MDA production, mitochondrial shrinkage, and reduced or absent cristae. Noni juice induces the accumulation of reactive oxygen species (ROS), elevated levels of malondialdehyde (MDA), mitochondrial contraction, and loss of cristae; these findings confirm that noni juice triggers ferroptosis in gastric cancer cells.

To further demonstrate that noni juice induces ferroptosis in gastric cancer cells, a rescue experiment was conducted using noni juice and a ferroptosis inhibitor. Five groups (PBS, 5% noni, 5% noni + Fer-1, 10% noni and 10% noni + Fer-1) were established using two gastric cancer cell lines. After 48 hours of treatment, proliferation was detected, lipid peroxidation levels were measured using the C11 BODIPY probe, and cellular iron ion content was determined by colorimetry, and the results are shown in Fig. 7. Through an EdU proliferation assay, it was found that cells treated with noni juice experienced varying degrees of death and decreased proliferation. However, after treatment with Fer-1, proliferation further increased, as shown in Fig. 7A. The lipid peroxidation levels of gastric cancer cells in each group after treatment were detected using the C11 BODIPY probe, as shown in Fig. 7B. Noni juice treatment elevated lipid peroxidation levels in gastric cancer cells, while the addition of Fer-1 reduced lipid peroxidation levels, indicating that Fer-1 can reverse the ferroptosis induced by noni juice. Downregulation of GPX4 leads to decreased clearance of lipid peroxides, causing oxidative stress accumulation and directly driving ferroptosis. The expression of GPX4 was studied using cellular immunofluorescence, as shown in Fig. 7C. Noni juice treatment induced a reduction in GPX4 expression in gastric cancer cells, while the addition of Fer-1 increased GPX4 expression, with a significant increase in the positive rate. Cellular iron ion content in gastric cancer cells was quantified using colorimetry, as shown in Fig. 7D. Noni juice treatment increased cellular iron ion content, which decreased after Fer-1 treatment, indicating that Fer-1 has a rescuing effect on ferroptosis in gastric cancer cells.

To investigate the safety of noni juice *in vivo*, H&E staining was performed on the liver and kidneys of mice. The results, as shown in Fig. 7E, revealed that following treatment with a dose of 25 mL kg^{-1} day^{-1}, no pathological changes were observed in the liver or kidneys. H&E staining of kidney tissues revealed well-preserved glomeruli and renal tubules both before and after treatment; similarly, no significant inflammation was detected in the liver. Immunohistochemical analysis of cancer tissues before and after animal intervention experiments further supported these findings. Differences in the positive expression rates of HO-1, GPX4 and Ki67 antibodies were observed. Following noni juice treatment, the expression levels of HO-1 were significantly elevated compared to the control group, and the expression levels of GPX4 and Ki 67 were significantly decreased compared to the control group, as shown in Fig. 7F. These results indicate that noni juice can modulate the growth of gastric cancer cells and promote ferroptosis in these cells.

Discussion

Research has found that key regulatory factors related to digestive system tumors, including *Helicobacter pylori* infection and transmission, are associated with the occurrence and development of gastric cancer, highlighting the critical role of ferroptosis in its treatment. Natural compounds including apigenin, quercetin, and curcumin have been found to have the potential to combat gastric cancer by inducing ferroptosis.[32] Plant compounds such as flavonoids, terpenes, and alkaloids inhibit system Xc^-, down regulate GPX4, and regulate iron metabolism, thereby inducing ferroptosis. Therefore, natural products or dietary components are important in inducing ferroptosis in gastric cancer.[33]

Noni exerts broad-spectrum anticancer effects through diverse molecular mechanisms. However, its relationship with GC has not been extensively studied. This research represents the first comprehensive investigation into the potential role of noni as a suppressor of GC cells in both *in vivo* and *in vitro* models. The study elucidates molecular mechanisms that are critical and novel in GC therapy. At the cellular level, the findings indicate that noni mediates ferroptosis in GC cells. This process involves iron-dependent phospholipid peroxidation and oxidative damage to cell membranes. The upregulation of HO-1 and the downregulation of GPX4 inhibit cysteine import, blocking the accumulation of phospholipid hydroperoxides (PLOOHs). This results in rapid and irreversible damage to the cell membrane, mitochondrial shrinkage, loss of cristae, increased membrane density, mitochondrial membrane rupture, altered levels of MDA and GSH, and an imbalance in the production and degradation of lipid-reactive oxygen species (ROS). Noni enhances the clearance of ROS and induces cell cycle arrest, thereby mitigating the initiation phase of carcinogenesis. It promotes apoptotic pathways, limit-

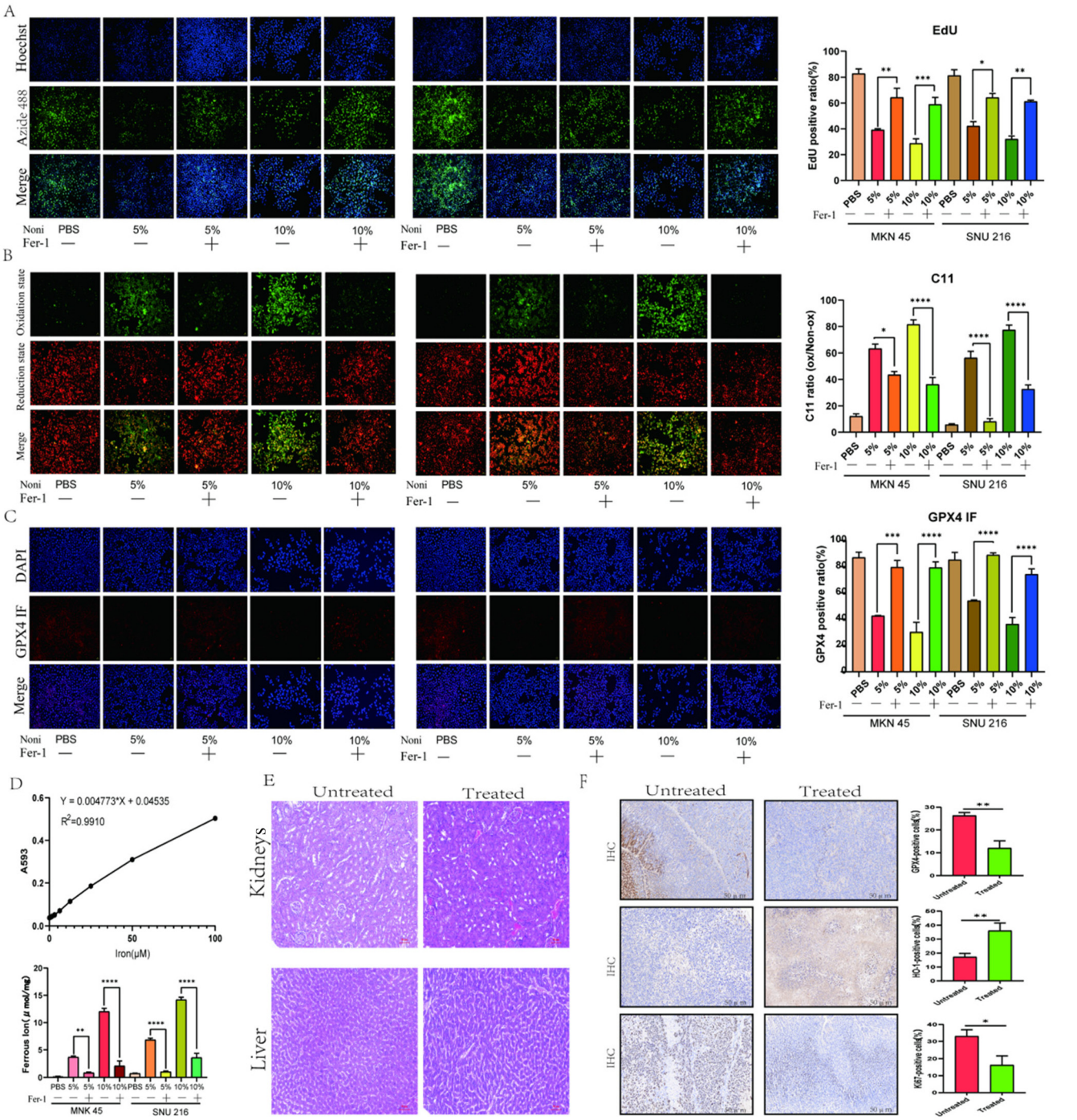

Fig. 7 Study on noni juice inducing ferroptosis in gastric cancer cells. (A) EdU cell proliferation (scale bar: 50 μm). (B) Representative images of C11-BODIPY immunofluorescence (scale bar: 50 μm). (C) Immunofluorescence images of GPX4 and DAPI (scale bar: 50 μm). (D) Detection of noni juice-induced ferrous ions in gastric cancer cells. (E) H&E staining of liver and kidney tissues in the mouse models (scale bar: 50 μm). (F) Immunohistochemical staining of HO-1, GPX4, and Ki67 in the mouse model. Data are presented as mean ± SD. Statistical significance is indicated as follows: *$p < 0.05$, **$p < 0.01$, ***$p < 0.001$ and ****$p < 0.0001$ compared to the control group.

ing tumor promotion. Additionally, noni reduces DNA damage and inhibits angiogenesis, cellular proliferation, and metastasis—processes that are pivotal in tumor progression. These changes collectively lead to ferroptosis, effectively controlling the progression of GC.[34–36]

This study concluded that the active components of noni influence mitochondrial function in GC cells and induce ferroptosis through the Nrf2/HO-1 signaling pathway. Furthermore, the active components affect the autophagic function of normal cells. Specifically, noni treatment signifi-

cantly decreased the proportion of G0/G1-phase cells by 25.66% and increased the proportion of S-phase cells by 76.57%. This alteration affected DNA synthesis, resulting in reduced GSH content, MDA accumulation, and mitochondrial damage. Treatment with ferroptosis inhibitors can further reverse this phenomenon. The active components of noni juice induce mitochondrial dysfunction, leading to the dissociation of Nrf2 and Keap1. This allows Nrf2 to translocate into the nucleus, resulting in the upregulation of HO-1 expression, which acts as an activator of ferroptosis. Consequently, MDA levels increase, ROS accumulate, GPX4 is depleted, and cellular oxidative phosphorylation and autophagy are disrupted. These changes also impact the expression of STAT3 and HIF1α, further contributing to the progression of ferroptosis. HO-1 has a "dual role" in ferroptosis, exhibiting antioxidant and cytoprotective effects under specific conditions, but when excessively activated, it may trigger ferroptosis by promoting iron release and iron overload. In this study, treatment with high concentrations of noni fruit extract represents sustained and intense stress stimuli, under which excessive or persistent activation of HO-1 may push cells toward ferroptosis. Nitti *et al.* reviewed the "double-edged sword" role of HO-1 in cell fate. Noni fruit is rich in bioactive components such as polysaccharides, flavonoids, cycloartanes, and organic acids.[37] The overall efficacy of its extracts is often not attributable to any single compound, but is more likely due to the complex synergistic effects among multiple components. The theoretical advantages of this synergy include multi-target effects, improved pharmacokinetics, reduced risk of drug resistance, balanced efficacy, and reduced toxicity. The study demonstrated that noni (*Morinda citrifolia* L.) fruits are more effective at stimulating immune responses than isolated polysaccharide components.[38] This provides a new idea for the treatment of GC using noni. In addition, the molecular mechanism of noni treating GC is *via* the Nrf2/HO-1 axis (Fig. 8). Nuclear factor erythroid 2-related factor 2 (Nrf2) is a stress-inducible transcription factor that undergoes degradation by Kelch-like ECH-associated protein 1 (Keap1). Upon dissociation from Keap1, Nrf2 translocates to the nucleus to initiate the transcription of antioxidant response element (ARE)-containing genes, such as heme oxygenase-1 (*HO-1*).[39]

In conclusion, this study demonstrated that the active components of noni induce ferroptosis in gastric cancer cells *via* the GPX4/HO-1 signaling pathway. However, further research is required to validate the mechanisms underlying the pharmacological effects of noni juice. This study highlights the potential therapeutic value of noni juice in GC treatment and deepens the understanding of its molecular mechanisms, contributing valuable insights for future cancer therapies. Additionally, the natural chemical composition, medicinal applications, and comprehensive utility of noni juice as a potent therapeutic agent for gastric cancer warrant further investigation. In many cancer treatments, ferroptosis often occurs simultaneously or sequentially with apoptosis, autophagy, and other forms of programmed cell death, forming a complex "death network". Ferroptosis may be one of the key

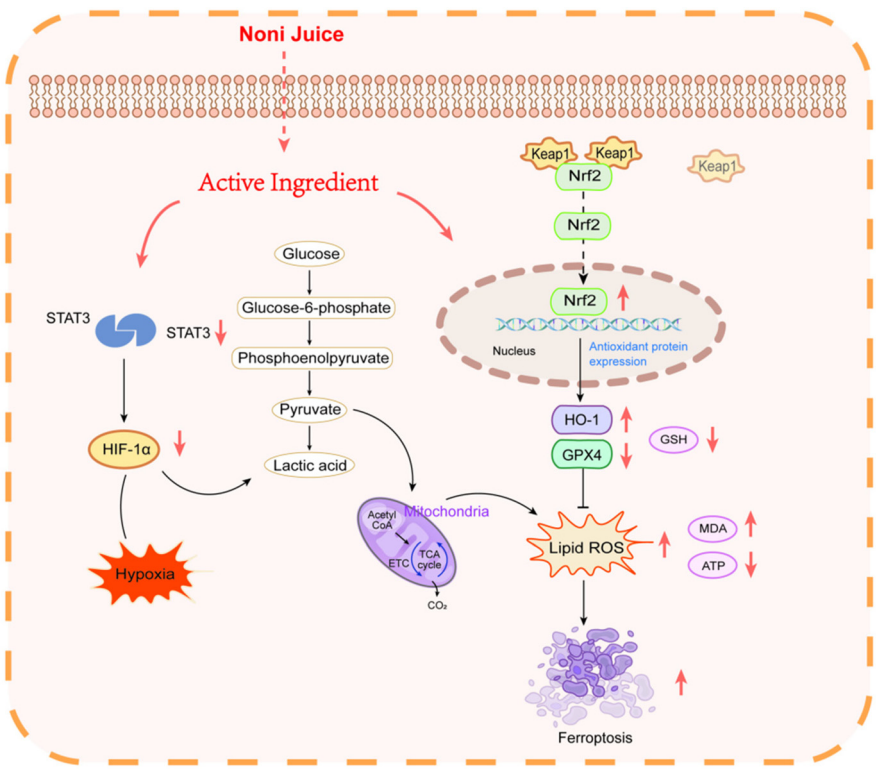

Fig. 8 The potential mechanism underlying the action of noni juice against GC.

mechanisms by which noni juice induces gastric cancer cell death, although other forms of cell death may also be involved in this process. This study aims to inhibit the development of gastric cancer at different stages by regulating, intervening in early gastric mucosal lesions, reversing precancerous lesions, and inducing cell apoptosis, autophagy, and ferroptosis.[40] Noni fruit can also be concentrated and freeze-dried using modern technology as a complementary therapy for tumors, and its feasibility as a daily dietary supplement supports the potential for clinical translational research.[41,42] Noni juice has the potential to become a nutritional supplement and a potential drug for cancer patients. The findings provide a theoretical foundation for the development and utilization of noni, highlighting the significant role of natural compounds in food for treating diseases.

Abbreviations

Fer-1	Ferrostatin-1
GSH	Glutathione
GPX4	Glutathione peroxidase 4
H&E	Hematoxylin–eosin
HO-1	Heme oxygenase-1
MDA	Malondialdehyde
MMP	Mitochondrial membrane potential
Nrf2	Nuclear factor erythroid 2-related factor 2
PBS	Phosphate-buffered saline
UPLC-Q Exactive MS	Ultra-high-performance liquid chromatography-quadrupole Exactive mass spectrometry
WB	Western blotting

Author contributions

Zhihao Xie: methodology, data curation, formal analysis, investigation, validation, visualization, supervision and writing – original draft preparation. Hejiao Li: software, formal analysis and investigation. Weifeng Lu and Lijie Liu: data curation and software. Dianxiao Liao: formal analysis, and validation. Chunmeng Mai: supervision. Xian Fu, Minni Zhang and Xiuying Tian: supervision, data curation and funding acquisition. Xinbao Hao and Lu Xu: conceptualization, methodology, resources, supervision, writing – review & editing and funding acquisition.

Conflicts of interest

The authors declare no conflict of interest.

Ethics approval and consent to participate

The ethics-related to experimental animals for this research has been approved by the Ethics Committee of Hainan Medical University, with the registration number HYLL-2024-108, HYLL-2023-378.

Data availability

The data that support the findings of this study are available from the corresponding author upon reasonable request.

Acknowledgements

The author(s) declare that financial support was received for the research and/or publication of this article. This work was supported by the Hainan Province Clinical Medical Center Construction Project ([2022]276), the Hainan Province Clinical Medical Center (QWYH2022341), the Hainan Provincial Natural Science Foundation of China (Grant No. 822QN468 and 821QN402), the Joint Program on Health Science & Technology Innovation of Hainan Province (Grant No. WSJK2024QN050, WSJK2024MS231, WSJK2025QN073 and WSJK2025QN099), and the Science and Technology Special Fund of Hainan Province, China, ZDYF2024SHFZ114.

References

1 E. C. Smyth, M. Nilsson, H. I. Grabsch, N. C. van-Grieken and F. Lordick, Gastric cancer, *Lancet*, 2020, **396**(10251), 635–648.
2 H. Sung, J. Ferlay, R. L. Siegel, M. Laversanne, I. Soerjomataram, A. Jemal, *et al.*, Global Cancer Statistics 2020: GLOBOCAN Estimates of Incidence and Mortality Worldwide for 36 Cancers in 185 Countries, *CA Cancer J. Clin.*, 2021, **71**(3), 209–249.
3 L. J. Yan, Y. F. Chen, T. Tao, Z. J. Hu, J. Z. Wang, J. W. You, *et al.*, Effect of Helicobacter pylori Eradication on Gastric Cancer Prevention: Updated Report From a Randomized Controlled Trial With 26.5 Years of Follow-up, *Gastroenterology*, 2022, **163**(1), 154–162.
4 J. W. J. Lee, F. Zhu, S. Srivastava, S. K. Tsao, C. Khor, K. Y. Ho, *et al.*, Severity of gastric intestinal metaplasia predicts the risk of gastric cancer: a prospective multicentre cohort study (GCEP), *Gut*, 2022, **71**(5), 854–863.
5 Q. Han, J. Shi, Y. Yu, H. Yuan, Y. Guo, X. Liu, *et al.*, Calycosin alleviates ferroptosis and attenuates doxorubicin-induced myocardial injury via the Nrf2/SLC7A11/GPX4 signaling pathway, *Front. Pharmacol.*, 2024, **15**, 1497733.
6 D. Yang, X. Yang, Y. Zhou, H. Wang and R. Wang, Fecal Microbiota Transplantation from Noni Fruit Phenolic-Rich Extract Intervention Mouse Donors Ameliorates Lipid Metabolism Disorder by Regulating the FXR-FGF15 Pathway in a Gut Microbiota-Dependent Manner, *J. Agric. Food Chem.*, 2025, **73**(28), 17672–17684.
7 H. C. Kumar, X. Y. Lim, F. H. Mohkiar, S. N. Suhaimi, N. M. Shafie and T. Y. C. Tan, Efficacy and Safety of

Morinda citrifolia L. (Noni) as a Potential Anticancer Agent, *Integr. Cancer Ther.*, 2022, **21**, 15347354221132848.

8 C. Zhang, C. H. Gu, M. R. Wang, J. X. Chen, H. D. Chang, Z. Q. Chang, *et al.*, Effect of temperature regulation on microbial community, volatile flavours, amino acid profiles, and iridoid glycosides during noni (Morinda citrifolia L.) fruit fermentation, *Food Chem.*, 2025, **462**, 140966.

9 X. A. Chen, C. H. Gu, K. X. Zhu, F. Xu, Z. Feng and Y. J. Zhang, Insight into the effects of different ripeness levels on the quality and flavor chemistry of Noni fruit (Morinda citrifolia L.), *Food Chem.*, 2024, **15**(434), 137408.

10 B. Kravić, T. Bionda, A. Siebert, P. Gahlot, S. Levantovsky, C. Behrends, *et al.*, Ubiquitin profiling of lysophagy identifies actin stabilizer CNN2 as a target of VCP/p97 and uncovers a link to HSPB1, *Mol. Cells*, 2022, **82**(14), 2633–2649.

11 C. W. Chee, N. H. Zamakshshari, V. S. Lee, I. Abdullah, R. Othman, Y. K. Lee, *et al.*, Morindone from Morinda citrifolia as a potential antiproliferative agent against colorectal cancer cell lines, *PLoS One*, 2022, **17**(7), e0270970.

12 Y. J. Zhou, X. T. Zhou, X. J. Huang, T. Hong, K. Zhang, W. C. Qi, *et al.*, Lysosome-Mediated Cytotoxic Autophagy Contributes to Tea Polysaccharide-Induced Colon Cancer Cell Death via mTOR-TFEB Signaling, *J. Agric. Food Chem.*, 2021, **69**(2), 686–697.

13 C. W. Chee, N. Mohd-Hashim and N. Nor-Rashid, Morindone as a potential therapeutic compound targeting TP53 and KRAS mutations in colorectal cancer cells, *Chem.-Biol. Interact.*, 2024, **392**, 110928.

14 A. Glaviano, A. S. C. Foo, H. Y. Lam, K. C. H. Yap, W. Jacot, R. H. Jones, *et al.*, PI3K/AKT/mTOR signaling transduction pathway and targeted therapies in cancer, *Mol. Cancer*, 2023, **22**(1), 138.

15 S. Jeyabalan, L. Bala, K. Subramanian, S. L. Jabaris, M. Sekar, L. S. Wong, *et al.*, Potential effects of noni (*Morinda citrifolia* L.) fruits extract against obsessive-compulsive disorder in marble burying and nestlet shredding behavior mice models, *Front. Pharmacol.*, 2022, **13**, 993927.

16 L. D. Ma, G. B. Lin, L. B. Yang, J. L. Cao, J. Wang, Q. D. Chen, *et al.*, Morinda citrifolia (Noni) Juice Suppresses A549 Human Lung Cancer Cells via Inhibiting AKT/Nuclear Factor-κ B Signaling Pathway, *Chin. J. Integr. Med.*, 2021, **27**(9), 688–695.

17 M. Guo, B. Y. Mao, F. A. Sadiq, Y. J. Hao, S. M. Cui, M. H. Yi, *et al.*, Effects of noni fruit and fermented noni juice against acute alcohol induced liver injury in mice, *J. Funct. Foods*, 2020, **70**, 103995.

18 G. Rajivgandhi, K. Saravanan, G. Ramachandran, J. L. Li, L. Yin, F. Quero, *et al.*, Enhanced anti-cancer activity of chitosan loaded Morinda citrifolia essential oil against A549 human lung cancer cells, *Int. J. Biol. Macromol.*, 2020, **164**, 4010–4021.

19 H. Yoshitomi, J. X. Zhou, T. Nishigaki, W. Li, T. H. Liu, L. L. Wu, *et al.*, Morinda citrifolia (Noni) fruit juice promotes vascular endothelium function in hypertension via glucagon-like peptide-1 receptor-CaMKKβ-AMPK-eNOS pathway, *Phytother. Res.*, 2020, **34**(9), 2341–2350.

20 K. Zhang, J. Meng, X. J. Li, X. Tang, S. H. Ma, Y. P. Lv, *et al.*, Noni (Morinda citrifolia L.) wine prevents the oxidative stress and obesity in mice induced by high-fat diet, *J. Food Biochem.*, 2020, **44**(11), e13460.

21 M. Y. Wang, Q. L. Wang, Q. Yang, X. X. Yan, S. X. Feng and Z. N. Wang, Comparison of Anthraquinones, Iridoid Glycosides and Triterpenoids in Morinda officinalis and Morinda citrifolia Using UPLC/Q-TOF-MS and Multivariate Statistical Analysis, *Molecules*, 2019, **25**(1), 160.

22 Y. Kim, J. Pyeon, J. Y. Lee, E. M. Kim, I. J. La, O. H. Lee, *et al.*, Chemical fingerprint analysis of fermented Morinda citrifolia L. (Noni) juice by UHPLC Q-TOF/MS combined with chemometric analysis, *Appl. Biol. Chem.*, 2024, **67**, 59.

23 Z. Sun, Z. Zhou, K. Liao, Y. Liu, Y. Liu, C. Wang, *et al.*, Polygala tenuifolia Willd. Extract delays non-alcoholic fatty liver disease progression in rats via the COX2 and PERK-elF2α-ATF4 pathway, *Front. Pharmacol.*, 2025, **16**, 1595752.

24 J. Y. Cai, Z. Ye, Y. Y. Hu, L. Ye, L. G. Gao, Y. X. Wang, *et al.*, Fatostatin induces ferroptosis through inhibition of the AKT/mTORC1/GPX4 signaling pathway in glioblastoma, *Cell Death Dis.*, 2023, **14**(3), 211.

25 J. B. Chen, X. F. Wang, X. D. Xin, Y. G. Zheng, F. G. Hou, C. H. Li, *et al.*, Comprehensive comparison of two colour varieties of Perillae folium by UHPLC-Q-TOF/MS analysis combining with feature-based molecular networking, *Food Chem.*, 2025, **463**(Pt 3), 141293.

26 D. Kitic, B. Miladinovic, M. Randjelovic, A. Szopa, V. Seidel, P. Prasher, *et al.*, Anticancer and chemopreventive potential of Morinda citrifolia L. bioactive compounds: A comprehensive update, *Phytother. Res.*, 2024, **38**(4), 1932–1950.

27 M. M. Liu, R. H. Ma, Z. J. Ni, K. Thakur, C. L. Cespedes-Acuña, L. Jiang, *et al.*, Apigenin 7-O-glucoside promotes cell apoptosis through the PTEN/PI3K/AKT pathway and inhibits cell migration in cervical cancer HeLa cells, *Food Chem. Toxicol.*, 2020, **146**, 111843.

28 X. R. Zhao, Z. Y. Wang, G. L. Wu, L. H. Yin, L. Xu, N. Wang, *et al.*, Apigenin-7-glucoside-loaded nanoparticle alleviates intestinal ischemia-reperfusion by ATF3/SLC7A11-mediated ferroptosis, *J. Controlled Release*, 2024, **366**, 182–193.

29 A. Pratas, B. Malhão, R. Palma, P. Mendonça, R. Cervantes and A. Marques-Ramos, Effects of apigenin on gastric cancer cells, *Biomed. Pharmacother.*, 2024, **172**, 116251.

30 C. Marrassini, L. Cogoi, V. Sülsen and C. Anesini, Apigenin-7-Glucuronide from Urera aurantiaca Inhibits Tumor Necrosis Factor Alpha and Total Nitrite Release in Lipopoly saccharide-Activated Macrophages, *J. Evidence-Based Complementary Altern. Med.*, 2020, 6638764.

31 R. J. Chen, Z. W. Jiang, Y. F. Cheng, J. Y. Ye, S. Z. Li, Y. T. H. Xu, *et al.*, Multifunctional iron-apigenin nanocomplex conducting photothermal therapy and triggering augmented immune response for triple negative breast cancer, *Int. J. Pharm.*, 2024, **655**, 124016.

32 X. Na, L. Li, D. Liu, J. He, L. Zhang and Y. Zhou, Natural products targeting ferroptosis pathways in cancer therapy, *Oncol. Rep.*, 2024, **52**(3), 123.

33 S. Liu, J. H. Chen, L. C. Li, Z. P. Ye, J. N. Liu, Y. H. Chen, *et al.*, Susceptibility of Mitophagy-Deficient Tumors to Ferroptosis Induction by Relieving the Suppression of Lipid Peroxidation, *Adv. Sci.*, 2025, **12**(6), e2412593.

34 Q. S. Lin, S. Li, H. J. Jin, H. Cai, X. Y. Zhu, Y. T. Yang, *et al.*, Mitophagy alleviates cisplatin-induced renal tubular epithelial cell ferroptosis through ROS/HO-1/GPX4 axis, *Int. J. Biol. Sci.*, 2023, **19**(4), 1192–1210.

35 Y. Liu, L. Wang, T. Huang, Y. Li and H. Zhang, Integrative Gut Microbiota and Metabolomic Analyses Reveal the PANoptosis- and Ferroptosis-Related Mechanisms of Chrysoeriol in Inhibiting Melanoma, *J. Agric. Food Chem.*, 2024, **72**(45), 25173–25185.

36 Y. Tang, Y. Zhuang, C. Zhao, S. Gu, J. Zhang, S. Bi, *et al.*, The metabolites from traditional Chinese medicine targeting ferroptosis for cancer therapy, *Front. Pharmacol.*, 2024, **15**, 1280779.

37 M. Nitti, S. Piras and L. Brondolo, Heme oxygenase 1 in the nervous system: does it favor neuronal cell survival or induce neurodegeneration?, *Int. J. Mol. Sci.*, 2018, **19**(8), 2260.

38 M. Ali, S. N. Manjula, I. Mohiuddin, K. Mruthunjaya, F. Shakeel, S. A. Mir, *et al.*, Noni enhances the anticancer activity of cyclophosphamide and suppresses myelotoxicity and hepatotoxicity in tumor-bearing mice, *J. Cancer Res. Clin. Oncol.*, 2024, **150**(4), 212.

39 W. X. Li, X. J. Yin, H. J. Fu, J. Y. Liu, Z. W. Weng, Q. Q. Mao, *et al.*, Ethanol extract of Eclipta prostrata induces multiple myeloma ferroptosis via Keap1/Nrf2/HO-1 axis, *Phytomedicine*, 2024, **128**, 155401.

40 W. Liao, J. Wang and Y. Li, Natural products based on Correa's cascade for the treatment of gastric cancer trilogy: Current status and future perspective, *J. Pharm. Anal.*, 2025, **15**(2), 101075.

41 Y. Guo, X. Chen, J. Hu, Y. Su, F. Yin and X. Liu, The dual role of SLC7A11 in tumor drug resistance: mechanisms, challenges, and therapeutic potential, *Am. J. Cancer Res.*, 2025, **15**(10), 4516–4532.

42 M. Guo, B. Y. Mao, F. A. Sadiq, Y. J. Hao, S. M. Cui, M. H. Yi, *et al.*, Effects of noni fruit and fermented noni juice against acute alcohol induced liver injury in mice, *J. Funct. Foods*, 2020, **70**, 103995.

